Cooling of medial septum reveals theta phase lag coordination of hippocampal cell assemblies

Peter Petersen[1] and György Buzsáki[1,2, 3,*]

Affiliations:

[1]Neuroscience Institute and [2]Department of Neurology Langone Medical Center, New York University, New York, NY 10016, USA

[2]Center for Neural Science, New York University, New York, NY 10003, USA

[3]Lead Contact

*Correspondence: gyorgy.buzsaki@nyumc.org

Summary

Hippocampal theta oscillations coordinate neuronal firing to support memory and spatial navigation. The medial septum (MS) is critical in theta generation by two possible mechanisms: either a unitary 'pacemaker' timing signal is imposed on the hippocampal system or it may assist in organizing subcircuits within the phase space of theta oscillations. We used temperature manipulation of the MS to confront these models. Cooling of the MS reduced both theta frequency and power, was associated with enhanced incidence of errors in a spatial navigation task, but did not affect the spatial map. MS cooling decreased theta frequency oscillations of place cells, reduced distance-time compression but preserved distance-phase compression of place field sequences within the theta cycle. We suggest that reciprocal MS-hippocampal communication is essential for sustaining theta phase-coordination of cell assemblies and, in turn, supporting its role in spatial memory.

Introduction

Theta frequency oscillations coordinate neuronal activity in the hippocampus-subicular-entorhinal complex and entrain neurons in various neocortical areas [1]. Damage or inactivation of the medial septum–diagonal band (MS) abolishes theta oscillations in all these areas [2,3] and is associated with impairment of memory, spatial navigation and other cognitive functions [4–8]. However, whether the behavioral impairment is due to silencing or damaging important septal afferents or to the absence of rhythmic coordination of activity in the hippocampal system has remained an unsolved challenge. Damaging or completely silencing the MS cannot distinguish between these competing alternative explanations. Perturbation studies using synchronizing electrical [9] (or optogenetic [10–12] stimulation is not effective to fully address this problem either because strong pulses impose global synchrony on all neurons unlike the situation under physiological conditions [13,14]. Therefore, we used temperature manipulation, an approach that is applicable to localizing the origin of temporal coordination [15]. Moderate local cooling does not interrupt local computation but alters multiple parameters of neurons from channel kinetics to transmitter release, resulting in an altered circuit dynamic [16–18]. For example, reducing temperature in the vocal center of the zebra finch resulted in the elongation of the song by proportionally slowing its acoustic microstructure [19].

By cooling the MS, we examined how slowing theta oscillations affect hippocampal network activity, physiological properties of neurons and their spatial correlates [20]. Several models assume that the phase interference between MS theta oscillation (LFP theta) and place inputs-driven faster oscillations of place cells and grid cells is the underlying mechanism of spike phase precession, a systematic shift of spike preference from the late to the early phase of theta oscillation, while the animal traverses the place field [12,21–25]. Since the rate of phase precession depends on the frequency difference between two oscillators, a prediction of this class of models is that the size of place fields should change but the fine temporal organization in the hippocampus will be preserved and, therefore, more assemblies can be packaged in a theta cycle (‘temporal coding’). An alternative hypothesis is that the fundamental organization in the septo-hippocampal system is not time- but phase-based, therefore theta cycle assembly organization should

remain unaltered but at the expense of affecting timing between place cell assemblies ('phase coding'; Figure 1). Because the integrity of theta oscillations has been linked to spatial memory [8,20], we also examined whether altering the time or phase dynamics would impair behavior.

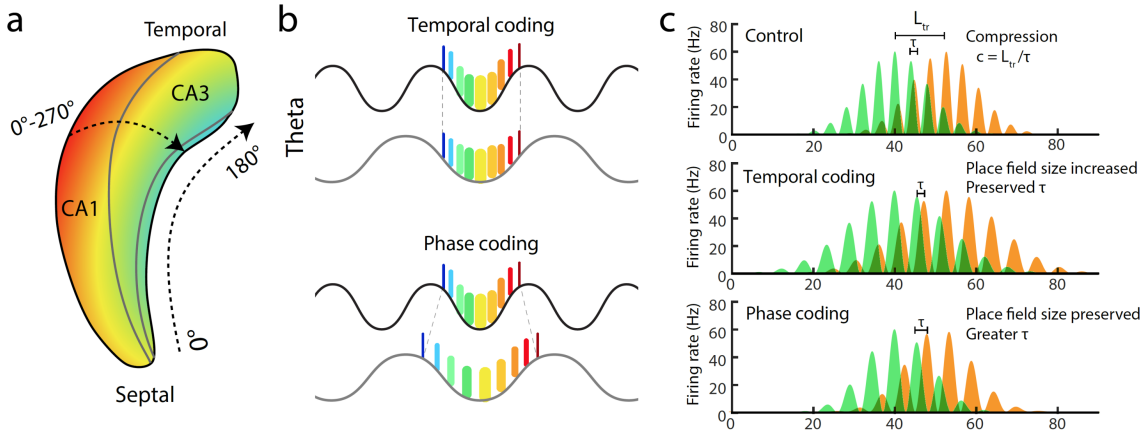

Fig. 1. **Theta phase dynamics and connectivity in the MS-hippocampal system**. **a**, Theta oscillation is a traveling wave and shows systematic phase shift in both the septo-temporal and CA1–CA3–dentate gyrus axes. Hippocampal neurons are not locked synchronously to a global theta rhythm but show a systematic phase shift up to 270º in the CA1-CA3-dentate gyrus axis and a gradual 180º shift from the septal to the temporal pole [13,14]. **b**, Hypothetical effects of MS cooling on within-theta neuronal assembly organization. Top: Time lags between place cells assemblies (different color ticks) remain unchanged with theta cycle lengthening (gray). Bottom: Place cells assemblies expand in time but keep their theta phase relationships. **c**, Theta cycle relationship between two overlapping place fields of the same size (L_{PF}). The travel distance (L_{tr}) between the peaks of the place fields is correlated with the time offset (τ) of spikes between the green and tangerine place neurons. The ratio of travel distance and theta time scale time lag defines distance to time compression ($c = L_{tr} / \tau$). Middle and bottom, Hypothetical effects of MS cooling with theta frequency decrease. Middle: Place field size changes but τ is preserved. Bottom: Fewer theta cycles occur within the same size place field and τ increases.

Results

MS cooling decreases hippocampal theta frequency and power

To achieve local cooling of the medial septum, we constructed a cryoprobe, consisting of a silver wire (125µm in diameter), graphene sheet, an air vacuum and a polyimide tubing (Fig. 2a; see Methods). The back end of the silver wire was coiled at the bottom of an insulated reservoir. Cooling was achieved by filling the reservoir with dry ice (−78.5º C). The protruding tip (1.5 mm) of the front-end wire was implanted into the medial septum-

diagonal band area (MS; Fig. 2b). A temperature sensor (k-type thermocouple; two 80µm wires) was attached to the outer surface of the cryoprobe cannula to continuously monitor local temperature (Fig. 2a; Suppl. Fig. 1). Pilot experiments were performed to perfect the device so that hippocampal theta frequency could be reduced for 5 to 15 min (n = 8 rats).

Using simultaneous temperature measurements in the MS and hippocampus, we found < 1.5^{o} C decrease in the hippocampus at the largest MS temperature decrease (16° C), that is within the physiological range of brain temperature (Suppl. Fig. 1f-j; [26]. Critically, in contrast to the rapid onset of cooling in MS (maximum effect at approximately 45 s; time constant: 11 sec), the mild temperature decrease in the hippocampus was considerably delayed (peak at 115 s; time constant 48s, right hippocampus, and 72 s left). Furthermore, the waveforms of action potentials in the hippocampus, a sensitive measure of temperature change [17,18], were not affected by MS cooling (Suppl. Fig. 1e).'

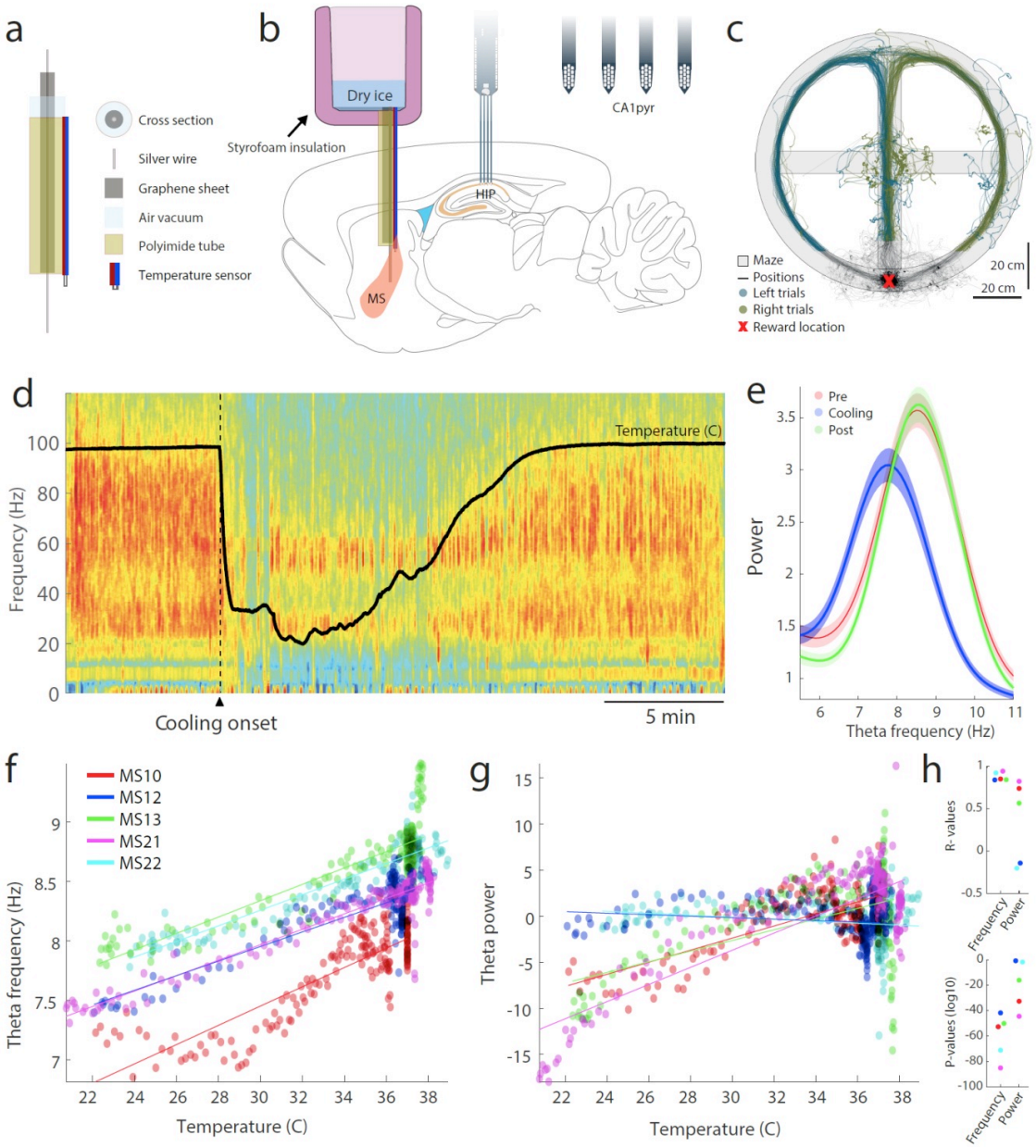

Fig. 2. **Cooling of MS affects theta oscillations**. **a**, Components of the cooling probe. **b**, Cooling probe and thermocouple are implanted in MS and silicon probes in the hippocampus. Dry ice is placed into the reservoir and MS is cooled by convection. **c**, Maze with left (blue) and right (green) run trajectories superimposed. **d**, Time-resolve wavelet spectrum before, during and after MS cooling (black line) in a single session. **e**, Theta frequency and power before and during MS cooling as a function of running speed (53 sessions in 5 rats). **f, g,** Effect of MS cooling on theta frequency (**f**) and power (**g).** Data from individual rats are shown separately by different colors. **h,** R and P values for theta frequency and power in individual rats.

In addition to the cooling probe, five rats were also implanted with multishank 64-site silicon probes bilaterally in the CA1 pyramidal layer of the dorsal hippocampus (Supplementary Material) and were trained in a figure-8 maze (spontaneous alternation task; Fig. 2b) to run for water reward. After a block of control trials (~ 40 trials), dry ice was placed into the reservoir, which reduced MS temperature for approximately 15 min (or corresponding to about 20 to 60 'cooling' trials), followed by recovery trials (20 to 80). MS cooling induced fast and reversible change in the frequency and power of hippocampal theta oscillations (Figure 2c, e, f). Theta frequency decreased linearly with MS temperature (down to 18-20° C; 0.81; P = 5.3610e-48) and this relationship was more consistent across animals than the effect on theta power (R = 0.54; P = 1.1846e-16; 0; Fig. 2g, h). The time course of theta frequency decrease, and less so its power, mirrored the temporal dynamic of MS cooling. Overall, these findings show that MS cooling had an immediate and strong effect on LFP theta and suggest that these changes were not a consequence of the spread of cooling to the hippocampus but due to altering the circuit dynamic within MS.

Effects of MS cooling on single neuron properties

MS cooling induced widespread but correlated physiological effects (Fig. 3). The theta oscillation frequency of pyramidal neurons decreased linearly and paralleled the downward frequency shift of LFP theta oscillation (Fig. 3a; f_{LFP}: R=0.66, Slope=0.071. f_p: R=0.38, slope=0.09). Theta frequency oscillation of putative fast spiking interneurons also decelerated (Suppl. Fig. 2d), commensurate with the downward frequency shift of LFP theta oscillation.

The range of within-field oscillation frequency of place cells (f_p) was approximately twice the range of LFP theta frequency within place fields (f_{LFP}; Fig. 3c). MS cooling decreased both f_p and f_{LFP}, measured within the place fields of neurons, by approximately the same degree (Fig. 3b,c; $f_{LFP\ pre}$=8.4±0.38, $f_{LFP\ cooling}$=7.7±0.36, $f_{LFP\ post}$=8.5±0.29; $f_{p\ pre}$=10.6±0.95, $f_{p\ cooling}$=9.5±0.84, $f_{p\ post}$=10.4±0.72, n=365). Both values recovered after cooling. The *y* intercepts of regression lines of the f_p versus f_{LFP} relationship shifted from pre-cooling to cooling but remained parallel to each other in each condition. The lines

connecting the centers of masses also remained largely parallel with the diagonal (Fig. 3c), indicating a preserved $f_p - f_{LFP}$ difference. Both within-field and peak firing rates of place cells decreased moderately during MS cooling (Suppl. Fig. 2; 11% and 12%; $P < 10^{-9}$ and $P < 10^{-11}$, respectively). Interneuronal firing rates also decreased by approximately the same degree (Suppl. Fig. 2). The slope of place cell spike – theta phase relationship ('phase precession' index; [25]) decreased slightly, but nevertheless significantly, during MS cooling (Fig. 3d).

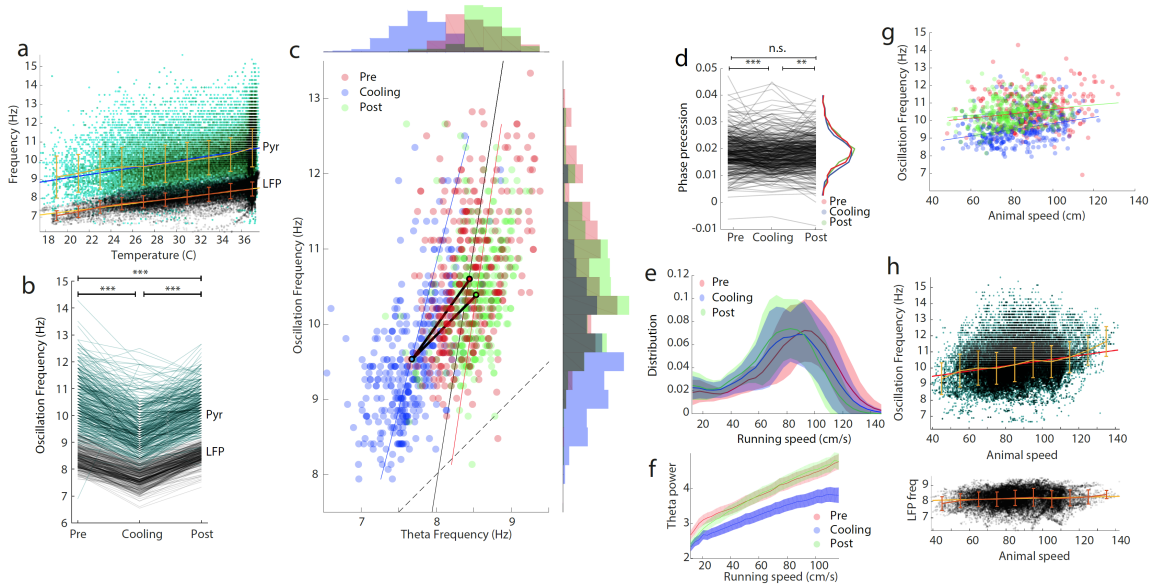

Figure 3. **Effects of MS cooling on single unit parameters**. **a**, LFP theta frequency (f_{LFP}) and oscillation frequency of pyramidal neurons (f_p) as a function of MS temperature. Each dot is a value measured in a single place field. Note parallel changes between f_p and f_{LFP}. **b**, Oscillation frequency shown separately for all place cells (f_p; gray) and LFP theta frequency (f_{LFP}; black) measured in the corresponding place fields before, during and after MS cooling. *** $P < 5.9e{-}8$ **c**, Correlation between LFP theta frequency (f_{LFP}) and place cell oscillation frequency (f_p; Pre R = 0.61; cooling R = 0.59; Post R = 0.36; $P < 2x10e{-}19$ each). Black lines connect the centers of mass of each cloud. Marginal histograms show the distribution of f_p of place cells and f_{LFP} in the corresponding place fields. Dashed line: diagonal. **d**, Theta phase precession slopes of place cell spikes before, during and after MS cooling. ** $P < 0.007$***; $P < 0.0003$. **e**, Distribution of running speeds in all sessions (N = 53). **f**, Theta power as a function of running speed. **g**, Place cell oscillation frequency (f_p) as a function of running speed, measured in each place field. **h**, f_p and f_{LFP} as a function of running speed. As in **g** but trials before, during and after MS cooling are pooled.

Since previous studies showed that the running speed of the animal is correlated with several physiological parameters [10,27,28], we aimed to disambiguate the effect of MS cooling and running speed. Running speed decreased relatively monotonically within session (Fig. 3e; see also Fig. 6c). The animal's speed correlated with both theta power and f_p (Fig. 3f, g). Yet, f_p changes during MS cooling could not be explained by decreased running velocity of the rat because f_p values during cooling were lower at all velocities (Fig. 3g). We examined the relation between running speed and LFP theta frequency (f_{LFP}) in two different ways. The first comparison was done on a trial basis, comparing the mean theta frequency with the mean running speed in each trial. This comparison showed a positive correlation before, during and after MS cooling with the largest changes taking place at lower running speeds (10 to 40 cm/s; Suppl. Fig. 2e). However, this comparison cannot dissociate the effect of speed from the effect of maze environment [29]. Therefore, we quantified speed – theta frequency relationship within each place field (f_{LFP}), together with the oscillation frequency of the corresponding place cell (f_p). This calculation revealed that while speed exerted a relatively linear effect on f_p, it had no or little effect on the frequency of f_{LFP} (Fig. 3h; [29,30] within the dominant speed range of the rat. As a result, the $f_p - f_{LFP}$ difference increased with running velocity. This is in contrast to the effect of MS cooling, after which the difference between f_p and f_{LFP} was preserved (Fig. 3a and c). Further, we examined all time delays between spikes of place cells in the same theta cycle and found that while their distributions remained unaltered between before and after MS cooling trials ($P = 0.75$, sign rank test), MS cooling increased theta cycle duration (Suppl. Fig. 4; $P<10^{-5}$, sign rank test). Overall, these findings indicate that the physiological effects of MS cooling are not confounded by a change in running speed.

Effect of MS cooling on place field features

In contrast to the described physiologic changes, spatial parameters of place fields were largely left unaffected by MS cooling. Place field size (L_{PF}) remained highly correlated before and after MS cooling (Fig. 4a, b; see Suppl. Fig. 4 for other place field features). L_{PF} and f_p were negatively correlated [25,31], and this relationship was not altered by

cooling, as illustrated by the similar slopes, even though the intercept of the regression line during cooling decreased (Fig. 4c, d).

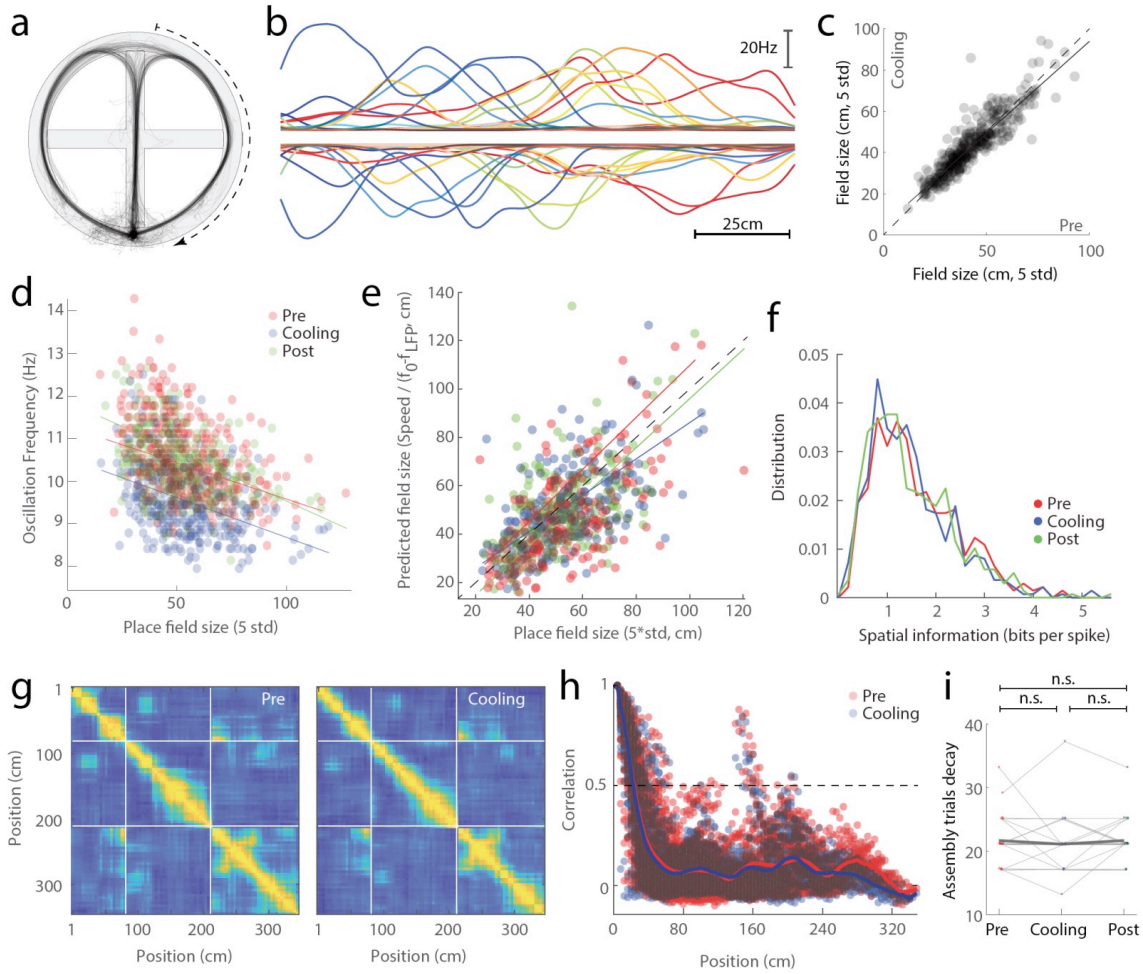

Fig. 4. **Place field features during by MS cooling**. **a,** Example of right arm runs in the T maze. **b**, Place fields in the right arm before (upward traces) and during MS cooling (downward traces) in a single session. Note preserved size, position and shape of place fields. **c**, Place field size does not change with MS cooling (R = 0.91). **d**, Place field size continues to be inversely correlated with f_p after MS cooling (before R = -0.49; cooling R -0.40; after R = 0.40. $P < 10^{-9}$ all conditions). **e**, Correlation between measured (x) and model-predicted (y) size of place fields before, during and after MS cooling. Place field size in the model [32] was derived from $S_{PF} = v/(f_p - f_{LFP})$. **f**, Information content of place cell spikes. None of the comparisons are significantly different (P > 0.26). **g**, Population vector cross-correlation matrices from a single session from baseline (pre-cooling) and MS cooling trials. White lines mark the boundary between central arm, right and left arms. **h**) Superimposed decorrelation curves for trials before and during MS cooling. To quantify the scale of the spatial representation, the interval at which the correlation dropped to 0.5 was calculated for each session. **i**) Decorrelations values for data from 21 sessions.

Next, we compared measured place field size with model-based calculations. Previous studies have demonstrated a quantitative relationship among theta frequency (f_{LFP}), oscillation frequency of pyramidal cells within their place fields (f_p), the duration it takes the rat to run across the place field (D_{PF}), place field size (S_{PF}) and the rat's velocity (v). Since $D_{PF} = 1/f_p - f_{LFP}$ [32] and D_{PF} can be calculated by dividing place field size (S_{PF}) with locomotion velocity within the place field ($S_{PF} = D_{PF}*v$), place field size is derived from $S_{PF} = v/(f_p - f_{LFP})$. We found a reliable and similar relationships between measured place field sizes and model-predicted sizes for trials before (R = 0.55), during (R = 0.54) and after (R = 0.11) MS cooling. Information content of place cell spikes was also left unaltered by MS cooling (P > 0.26).

We also investigated potential changes to the scale of distance representation at the population level resulting from MS cooling. We calculated the correlations between pairs of population vectors of unit firing constructed from binned rate maps [33]. The distance in maze corridor bins at which the spatial population vector correlation function dropped to 0.5 was used as a measure of the scale of the spatial representation, that is independent of any definition of place field. Population vector correlation of place cells was not affected by MS cooling (Fig. 4g, h). This analysis further suggested that spatial representation by place cell population was largely unaffected by MS cooling (Fig. 4i).

MS temperature effects on theta phase/time compression of place cells sequences

Our findings so far revealed a contrast between consistent changes in physiological parameters of single neurons and the stability of their place field features by MS cooling. Because spatial features do not inform us about the contribution of theta oscillations to the dynamic properties of place cells, we next examined the temporal sequences of place cell assemblies in the theta cycle (Fig. 5a, b). The distances between place cell peaks (L_{tr}) are known to correlate with their theta-scale time lags (τ) and phase lags, and the ratio of L_{tr} and τ is known as distance-time compression (c; Figure 1a; [27,28,32,34–36]). To display the dynamics of ensemble compression of place cell distances as the animal passes through sequential positions in the maze, we plotted the sequence compression for the entire

population of place cell pairs over several theta cycles within a 0.8-s period. In Fig. 5c, each dot corresponds to the time difference of spike occurrences of place neuron pairs (τ), averaged across all trials of a session (n = 18 sessions in 5 rats). This representation mimics the spatial-temporal evolution of spiking of all pyramidal neurons in the dorsal hippocampus as the rat traverses the place field center of a reference neuron [34]. The ‘‘clouds’’ are spaced by theta-scale intervals, relating to the joined oscillating frequency of place cell pairs and the slope corresponds to the distance-to-theta scale-time compression (*c;* [37]. Several place cells are active together in each theta cycle, but the group composition varies from cycle to cycle (Fig. 5b; [34,38].

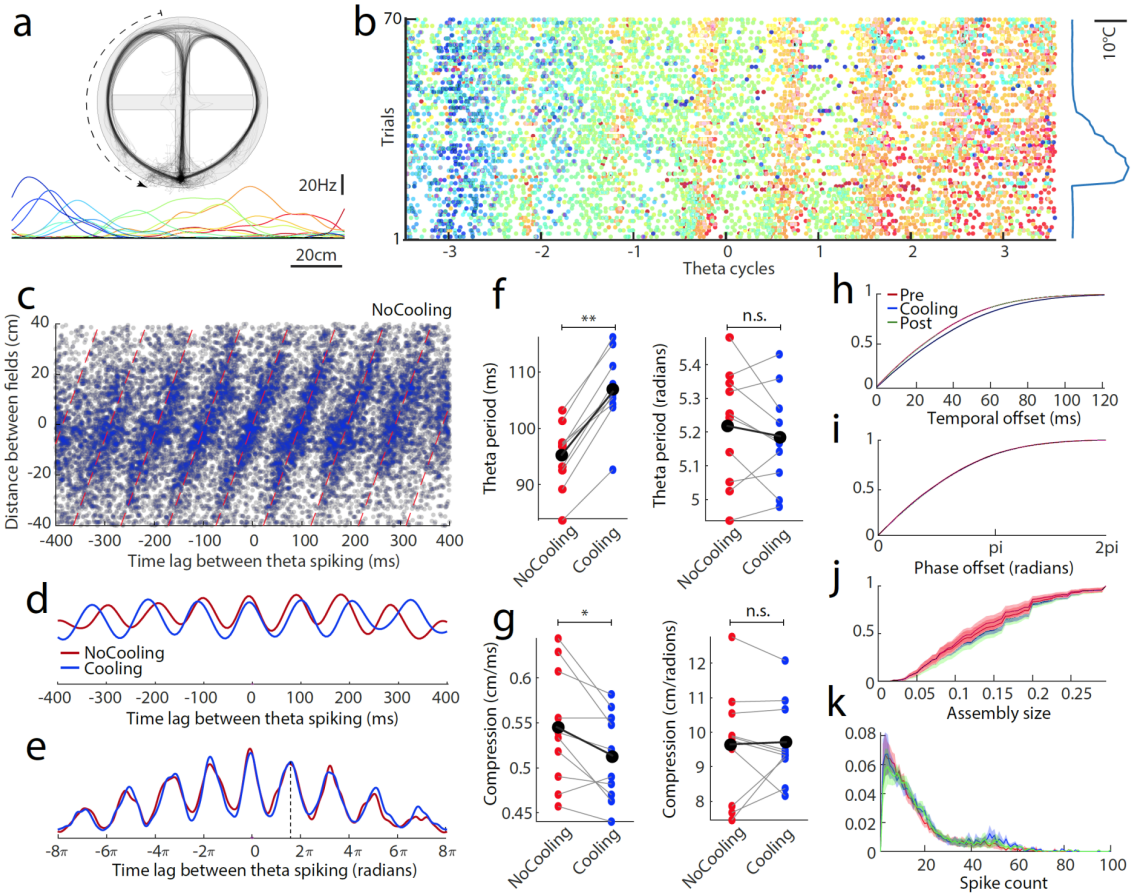

Figure 5. **Distance–theta time scale compression is affected by MS cooling**. **a**, Selected place fields in the left arm of the maze before MS cooling in a single session. **b**, Within-theta cell assemblies. Each row of dots is a trial of the spiking activity of place cells (same color code as in **a** in successive theta cycles). 0 is the theta cycle in the middle of the left arm. Note shifting cell assemblies in successive theta cycles (from blue to red) and preserved phase preference of place cell spikes during and after MS cooling (right trace). **c**, Relationship between distances of place field peaks across neuron pairs and their theta time lags prior to MS cooling. Each dot corresponds to a neuron pair between the peaks of place fields vs. theta-scale time lag (τ; 2948 = pairs across 18

sessions, 5 rats). Red dashed line; compression index, c = 0.54 cm/ms). **d**, Summed activity of the theta repeated cross-correlograms (as in **c**) before and during MS cooling. **e**, Similar to **d** but instead of time lags, within-theta phase lags between spikes were calculated. Vertical dashed line indicates that the oscillation frequency of the spike cross-correlations is faster than that of LFP theta (2π). **f**, The duration of the theta-repeated spike cross-correlograms significantly increased during MS cooling, compared to control (Pre and Post-cooling epochs combined) trials (** P = 0.002; two-sided signed rank test), whereas the phase-lag repetitions remained unaffected (n.s., P = 0.32). **g**, The compression index, c (cm/ms) significantly decreased during MS cooling (* P = 0.02) but the distance/phase lag compression (cm/radian) remained unaffected (P = 0.92). **h**, Cumulative distributions of theta scale time lags (τ) between place cell pairs before (Pre), during and after (Post) MS cooling. MS cooling data are significantly different from both Pre- and Post-cooling trials (Pre vs cooling P = 8.0^{-5}; Post vs cooling P = 0.00032; N = 10 sessions, 4 rats). Pre and post-cooling curves are strongly superimposed (Pre vs Post P = 0.79). **i**, Same as in **h**, but for phase lags (all comparisons are non-significant, P > 0.24). **j**, Cumulative plots of the fraction of all simultaneously recorded neurons active in the theta cycle (before vs cooling P = 0.28; after vs cooling P = 0.006; before vs after P = 0.0005). **j**, Distribution of spike counts within theta cycles (before and after are not different from MS cooling; P > 0.058).

Both the joined oscillating frequency of place cell pairs and c were affected by MS cooling (Fig. 5d,f,g). Because the compression index also depends on running speed [38] and because running speed gradually decreased across the entire session (Fig. 3e; 6c), we combined trials before and after cooling into a single control group. During MS cooling, $1/f_p$ increased (i.e., f_p decreased) in each examined session relative to control runs (Fig. 5f, g; 0.002; Wilcoxon signed rank test), whereas distant-time compression decreased (Fig. 5g; P = 0.02). We also constructed analogous plots displaying L_{tr} versus theta phase lags of spike pairs, instead of time lags. Phase lags remained unchanged after cooling (Fig. 5f; P > 0.24 for all pairs; Wilcoxon signed rank test) and, as a consequence, the ratio (i.e., L_{tr} versus theta 'phase compression') between L_{tr} and phase lag did not change either (P < 0.92; Fig. 5g).

Because distances between place field peaks (L_{tr}) were not affected by MS cooling (Fig. 4c and g-i) but distance-time compression decreased (Fig. 5g), time lags (τ) are expected to increase. To examine this effect directly, we plotted the distributions of both theta time lags (τ) and phase lags between all pairs of place cells in each session. During MS

cooling, the time lags increased significantly (Fig. 5h; $P < 10^{-4}$; sign rank test; n = 10 sessions), whereas they were not different from each other during precooling and post-cooling sessions (P = 0.79). In contrast, phase lags between spikes of place cell pairs were not affected by MS cooling (Fig. 5i; P > 0.24 between all conditions). Thus, theta phase lags remained similar while time lags increased.

These findings suggested that the same number of place cell assemblies were compressed into theta cycles after MS cooling and the assemblies were proportionally dispersed within the lengthened cycle (Fig. 5c,d). In support of this hypothesis, we found that the fraction of place cells active in a given theta cycle was not significantly affected by MS cooling (Fig. 5j; P = 0.2). The number of spikes emitted by all neurons per theta cycle was also preserved after MS cooling (Fig. 5k), which might be explained by the similar magnitude of the within-field firing rate decrease of place cells (~12%; Supplementary Fig. 2) and theta frequency decrease (~12%; Fig. 3a and b).

MS cooling increases behavioral errors

In light of the altered relationship between spatial correlates of place cells and their physiological organization, brought about by MS cooling, we next examined how such dissociation affected spatial memory. The temperature decrease in the MS was immediately accompanied by increased choice errors in the maze (Fig. 6a-c). The worst memory performance occurred between trials 4 and 8 after MS cooling, when the MS temperature reached its minimum, accompanied by the largest decreases of theta frequency and power (Fig. 6c; see also Suppl. Fig. 5). Overall, the number of memory errors increased approximately 3-fold, assessed either within rats (P < 0.05 for all animals) or for all animals (P = 10e-6; Fig. 6d, e). The incidence of errors negatively and significantly correlated with temperature change (R = – 0.35; P < 0.01; all animals), theta frequency (R = – 0.35; P < 0.01; all animals) and less so with theta power (2 of 5 animals had significant R > – 0.3; P < 0.01) and not with the running speed of the rat (R ~ 0.1; P > 0.05 for all animals; Figure 6f-j).

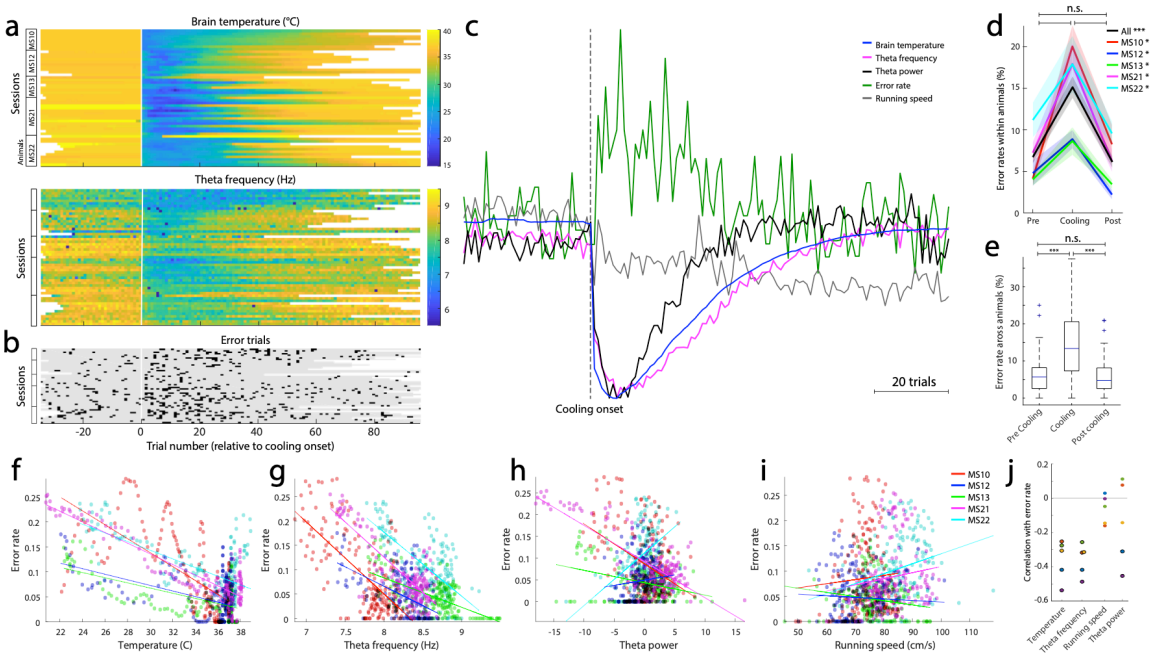

Figure 6. **Effects of MS cooling on behavior**. **a**, MS temperature (top) and theta frequency shift (bottom) as a function of trial number. Each line corresponds to a single session. Animal IDs are indicated on the left. Vertical line marks the onset of cooling. **b**, Incidence of error trials. **c**, Time courses of MS temperature, theta frequency, power and running speed (mean of all sessions). Note tight correlation between MS temperature, theta frequency and power. In contrast, speed shows a monotonic function across trials. **d**, Choice errors shown separately for each animal. Standard errors are shown in shaded colors. Black line, group means. * P < 0.05; *** P = 10e-6. **e**, Choice errors shown as boxplots constructed from all sessions. ** P < 10e-7. ns = nonsignificant. **f-i**, Relationship between memory errors and temperature (**f**), theta frequency (**g**), theta power (**h**) and running speed (**i**). **j**, Correlation values between memory errors and parameters shown in **f** to **i** for each rat. Significant values indicated by black circles (P < 0.05). Same color indicates same animal.

Discussion

Cooling the MS reduced both LFP theta frequency and power in the hippocampus, associated with enhanced incidence of errors in a spatial navigation task without affecting spatial attributes of individual place cells and the spatial map. The slowing of LFP theta oscillation was paralleled with a commensurate decrease of theta frequency oscillation of place cells, reduced time compression but largely preserved phase compression of place field sequences within theta cycles and subtle decrease of firing rates of both pyramidal cells and interneurons.

Mechanisms of MS-hippocampal theta oscillations

Early experiments suggested that the MS acts as a 'pacemaker', sending out synchronous outputs, akin to a conductor of an orchestra [1,2,12,22,39,40]. An alternative model is based on the reciprocal relationship between MS and the hippocampus [41]. In one direction, MS GABAergic neurons innervate hippocampal and entorhinal interneurons [42–46]. In the return direction, long-range GABAergic neurons send axons to the MS [47,48].

Interneurons, populations of pyramidal cells and MS neurons all fire at the frequency of hippocampal LFP [32,36,49]. In contrast, active individual pyramidal cells and granule cells oscillate faster (f_p) than the population activity (f_{LFP}), resulting in phase interference and measured experimentally by the 'phase precession' slope [25]. The oscillation frequency of place cells is inversely correlated with their phase-precession slope and the place field size ($L_{PF} = v/(f_p - f_{LFP})$; [32], where v is the velocity of the animal. We found that at faster velocities the difference between f_p and f_{LFP} increases, which may explain the place field size invariance [28,50].

If the sole function of MS were to supply a pacemaker pattern by entraining target interneurons in the hippocampus [42] at LFP frequency then slowing the output MS theta frequency would result in a larger $f_p - f_{LFP}$ difference and, consequently steeper phase precession and smaller place fields [12,22,37]. However, during MS cooling f_p and f_{LFP} decreased proportionally (i.e., $f_p - f_{LFP}$ difference remained constant) and the influence of the rat's running velocity on f_p was preserved (Fig. 3a, c). These preserved relationships can explain why place field size was not affected by MS cooling.

The travel distances between the peak positions of place cell sequences (L_{tr}) are correlated with their theta-scale time lags (τ) and phase lags, and the ratio of travel distance and theta-scale time lag (L_{tr}/τ) is known as distance-to-time compression (c; [34,37]). This distance-to-duration compression is believed to be the mechanism that chains together evolving cell assemblies, and explains the succession of place fields during navigation emerging from place cell sequences within theta cycles (τ; [7,22,34,51–54]. Place field sizes (L_{PF}) and the distances between place field peaks (L_{tr}) were not affected by MS

cooling. On the other hand, the theta-scale time lags (τ) between successive place cell assemblies increased. As a result, the compression index (*c*) decreased. In contrast, phase lags between successive place cells within the theta cycle were not affected. These findings suggest that the fundamental organization of cell assemblies in the hippocampus is based on theta phase-preservation mechanisms, even at the expense of longer temporal lags between assemblies.

What are the mechanisms that keep the phase-organization within the MS-hippocampus loop when theta frequency changes? Sequential activation of pyramidal neurons can, in principle, be controlled either by environmental signals [55] or internally generated mechanisms [54]. Following pharmacological inactivation of the MS, internally generated sequences disappear and theta-scale timing of place cells is impaired without affecting place cell positions on the [7]. A previous experimental-computational model has shown that temporal lags between assemblies (τ) are correlated with the duration of the theta cycle [32], but the physiological mechanism of the delays (τ) has remained undisclosed. One possibility is that the delays are a consequence of inhibition between competing successive cell assemblies. Under this hypothesis the currently active assembly 'enslaves' a set of interneurons, which in turn, provide recurrent inhibition as well as suppresses the competing cell assemblies [28]. This mechanism is supported by intracellular observations showing that the frequency of membrane potential fluctuation in the soma, reflecting largely the activity of perisomatic inhibition [56], is identical with the spike oscillation frequency of the recorded place neuron (f_p; [23]. Furthermore, fast firing, putative perisomatic interneurons often show the same phase precession slopes as their monosynaptically driving place cells [28,37]. Thus, a given neuronal assembly 'coding' for a given place suppresses other assemblies by transiently enslaving perisomatic interneurons. According to this framework, the competitive mechanisms responsible for the delays between cells assemblies may reside in hippocampal circuits [32]. However, the current findings demonstrate that the MS plays a critical role in adjusting the theta phase delays between neighboring place fields of pyramidal cells. A putative mechanism may involve the reciprocal circuit between GABAergic neurons in MS and hippocampus. MS parvalbumin-expressing neurons innervate a variety of inhibitory neuron types in the

hippocampus [42] and entorhinal cortex [5,43,44,57,58], while cholinergic neurons affect both principal cells and interneurons [46]. In turn, long-range hippocampo-septal interneurons inhibit MS neurons [45,47,48]. These hippocampo-septal inhibitory neurons are likely be of special importance because they are the best candidate for integrating the activity of multiple place cell assemblies and feedback population theta-oscillatory pulsing to subgroups of MS neurons.

Local neuron assemblies in the septo-temporal and subiculo-fimbrial axes of the hippocampus and in the dorsovental axis of the entorhinal cortex discharge at different times/phases related to the reference LFP theta signal (Fig. 1a; [13,14]. This mosaic-like phase organization and feedback can explain why the MS neuronal populations span their firing preference to the entire phase range of the theta cycle [59], possibly assisted by local inhibitory interactions among the MS GABAergic population. Thus, instead of a unitary 'pacemaker', we hypothesize that the MS neurons form myriads of topographically organized reciprocal circuits with multitudes of local oscillating neuronal assemblies in the hippocampal-entorhinal system. The advantage of multiple reciprocal subcircuits is that by bringing together variable phase representations from the large hippocampal space into the small volume of MS would allow to set delays among the MS GABAergic population and produce a coherent but phase-shifted theta waves throughout the hippocampal system, despite the vastly different oscillation frequencies and phase preferences of neurons.

MS cooling-induced memory impairment

MS cooling exerted a robust effect on spatial memory, comparable to damage or pharmacologic inactivation of MS [60,61]. Unlike neuron-specific manipulations [8,11,12,62], local cooling affects all neurons in MS and possibly its surrounding structures. Therefore, one possible interpretation of the behavioral effects is that moderate cooling of LS and/or anterior end of the hippocampus is responsible for the behavioral deficit. However, lesion of LS does not have an impact on spatial behavior [6,8,63,64]. Furthermore, previous studies have shown that decreasing brain temperature even down to 30° C was not sufficient to impair spatial navigation in rats [26,65]. In humans, cognitive functions are not affected

until the brain is cooled to about 33°C [66]. Thus, moderate cooling of the structures surrounding the septum may not fully account for the observed severe memory deficit. More importantly, choice errors correlated best with the temporal dynamic of MS cooling and the largest memory deficit was observed at the maximum temperature drop and theta frequency drop decrease, tens of seconds before cooling affected the hippocampus.

Despite the seemingly subtle but multiple changes of physiological parameters, choice errors increased almost three-fold during MS cooling. LFP theta frequency decreased by 12 % and within-field firing rates of place cells decreased by a similar proportion (12%; interneurons 14%). This can explain why the fraction of place cells and the number of spikes within theta cycles were largely unaffected by MS manipulation. Cooling, therefore, exerted its main physiological effect by dispersing the same number of cell assemblies within the phase space of the prolonged theta cycles (Fig. 1b), as demonstrated by the longer τ in the face of preserved phase differences between place field peaks. During MS cooling, the same segment of the environment is 'represented' by the same number of neuronal assemblies but repeated fewer times due to the prolonged theta cycle and with longer time offsets between successive assemblies.

One possible explanation of the memory impairment is that MS cooling did not affect all neurons in the medial septum/diagonal band equally, thereby bringing about variable timing effects along the septo-temporal axis of the hippocampus or between hippocampus, entorhinal cortex and partner structures. Alternatively, downstream reader structures, presumably not part of the MS-controlled theta system, failed to interpret the temporally changed hippocampal messages [67]. Overall, our findings suggest that the fundamental organization scheme in the septo-hippocampal system is phase-based and that even minuscule temporal changes of assembly organization can bring about behavioral consequences.

Reference list

1. Buzsáki, G. Theta Oscillations in the Hippocampus. *Neuron* **33**, 325–340 (2002).

2. Petsche, H., Stumpf, C. & Gogolak, G. The significance of the rabbit's septum as a relay station between the midbrain and the hippocampus I. The control of hippocampus arousal activity by the septum cells. *Electroen Clin Neuro* **14**, 202–211 (1962).

3. Vertes, R. & Kocsis, B. Brainstem-diencephalo-septohippocampal systems controlling the theta rhythm of the hippocampus. *Neuroscience* (1997).

4. Brandon, M. P. *et al.* Reduction of Theta Rhythm Dissociates Grid Cell Spatial Periodicity from Directional Tuning. *Science* **332**, 595–599 (2011).

5. Jeffery, K. J., Donnett, J. G. & O'Keefe, J. Medial septal control of theta-correlated unit firing in the entorhinal cortex of awake rats. *Neuroreport* **6**, 2166–2170 (1995).

6. Leutgeb, S. & Mizumori, S. J. Excitotoxic Septal Lesions Result in Spatial Memory Deficits and Altered Flexibility of Hippocampal Single-Unit Representations. *J Neurosci* **19**, 6661–6672 (1999).

7. Wang, Y., Romani, S., Lustig, B., Leonardo, A. & Pastalkova, E. Theta sequences are essential for internally generated hippocampal firing fields. *Nat Neurosci* **18**, 282–288 (2015).

8. Winson, J. Loss of hippocampal theta rhythm results in spatial memory deficit in the rat. *Science* **201**, 160–163 (1978).

9. McNaughton, N., Ruan, M. & Woodnorth, M.-A. Restoring theta-like rhythmicity in rats restores initial learning in the Morris water maze. *Hippocampus* (2006).

10. Dannenberg, H. *et al.* The Firing Rate Speed Code of Entorhinal Speed Cells Differs across Behaviorally Relevant Time Scales and Does Not Depend on Medial Septum Inputs. *The Journal of neuroscience : the official journal of the Society for Neuroscience* (2019).

11. Vandecasteele, M. *et al.* Optogenetic activation of septal cholinergic neurons suppresses sharp wave ripples and enhances theta oscillations in the hippocampus. *Proc National Acad Sci* **111**, 13535–13540 (2014).

12. Zutshi, I. *et al.* Hippocampal Neural Circuits Respond to Optogenetic Pacing of Theta Frequencies by Generating Accelerated Oscillation Frequencies. *Current biology : CB* (2018).

13. Lubenov, E. V. & Siapas, A. G. Hippocampal theta oscillations are travelling waves. *Nature* (2009).

14. Patel, J., Fujisawa, S., Berényi, A., Royer, S. & Buzsáki, G. Traveling Theta Waves along the Entire Septotemporal Axis of the Hippocampus. *Neuron* **75**, 410–417 (2012).

15. Fee, M. S. & Long, M. A. New methods for localizing and manipulating neuronal dynamics in behaving animals. *Current Opinion in Neurobiology* (2011).

16. Katz, P. S., Sakurai, A., Clemens, S. & Davis, D. Cycle period of a network oscillator is independent of membrane potential and spiking activity in individual central pattern generator neurons. *Journal of Neurophysiology* (2004).

17. Thompson, S., Masukawa, L. & Prince, D. Temperature dependence of intrinsic membrane properties and synaptic potentials in hippocampal CA1 neurons in vitro. *Journal of Neuroscience* (1985).

18. Volgushev, M., Vidyasagar, T., Chistiakova, M., Yousef, T. & Eysel, U. Membrane properties and spike generation in rat visual cortical cells during reversible cooling. *Journal of Physiology-London* (2000).

19. Long, M. A. & Fee, M. S. Using temperature to analyse temporal dynamics in the songbird motor pathway. *Nature* (2008).

20. O'Keefe, J. & Nadel, L. The Hippocampus as a Cognitive Map. *Q Rev Biology* **55**, 98–98 (1980).

21. Burgess, N., Barry, C. & O'Keefe, J. An oscillatory interference model of grid cell firing. *Hippocampus* (2007).

22. Chadwick, M. J. *et al.* Semantic representations in the temporal pole predict false memories. *Proc National Acad Sci* **113**, 10180–10185 (2016).

23. Harvey, C. D., Collman, F., Dombeck, D. A. & Tank, D. W. Intracellular dynamics of hippocampal place cells during virtual navigation. *Nature* (2009).

24. Kamondi, A., Acsady, L., Wang, X. & Buzsaki, G. Theta oscillations in somata and dendrites of hippocampal pyramidal cells in vivo: activity-dependent phase-precession of action potentials. *Hippocampus* (1998).

25. O'Keefe, J. & Recce, M. L. Phase relationship between hippocampal place units and the EEG theta rhythm. *Hippocampus* **3**, 317–330 (1993).

26. Moser, E. & Andersen, P. Conserved spatial learning in cooled rats in spite of slowing of dentate field potentials. *Journal of Neuroscience* (1994).

27. Diba, K. & Buzsaki, G. Hippocampal network dynamics constrain the time lag between pyramidal cells across modified environments. *The Journal of neuroscience : the official journal of the Society for Neuroscience* (2008).

28. Geisler, C., Robbe, D., Zugaro, M., Sirota, A. & Buzsáki, G. Hippocampal place cell assemblies are speed-controlled oscillators. *Proc National Acad Sci* **104**, 8149–8154 (2007).

29. Montgomery, S. M., Betancur, M. I. & Buzsaki, G. Behavior-dependent coordination of multiple theta dipoles in the hippocampus. *The Journal of neuroscience : the official journal of the Society for Neuroscience* (2009).

30. Czurko, A., Hirase, H., Csicsvari, J. & Buzsaki, G. Sustained activation of hippocampal pyramidal cells by 'space clamping' in a running wheel. *European Journal of Neuroscience* (1999).

31. Dragoi, G. & Buzsaki, G. Temporal encoding of place sequences by hippocampal cell assemblies. *Neuron* (2006).

32. Geisler, C. *et al.* Temporal delays among place cells determine the frequency of population theta oscillations in the hippocampus. *Proc National Acad Sci* **107**, 7957–

7962 (2010).

33. Gothard, K., Skaggs, W. & McNaughton, B. Dynamics of mismatch correction in the hippocampal ensemble code for space: interaction between path integration and environmental cues. *Journal of Neuroscience* (1996).

34. Dragoi, G. & Buzsaki, G. Temporal encoding of place sequences by hippocampal cell assemblies. *Neuron* (2006).

35. Ego-Stengel, V. & Wilson, M. A. Spatial selectivity and theta phase precession in CA1 interneurons. *Hippocampus* (2007).

36. Gothard, K., Skaggs, W. & McNaughton, B. Dynamics of mismatch correction in the hippocampal ensemble code for space: interaction between path integration and environmental cues. *Journal of Neuroscience* (1996).

37. Maurer, A. P., Cowen, S. L., Burke, S. N., Barnes, C. A. & McNaughton, B. L. Organization of hippocampal cell assemblies based on theta phase precession. *Hippocampus* (2006).

38. Maurer, A. P., Burke, S. N., Lipa, P., Skaggs, W. E. & Barnes, C. A. Greater running speeds result in altered hippocampal phase sequence dynamics. *Hippocampus* **22**, 737–747 (2012).

39. Borhegyi, Z., Varga, V., Szilágyi, N., Fabo, D. & Freund, T. F. Phase Segregation of Medial Septal GABAergic Neurons during Hippocampal Theta Activity. *J Neurosci* **24**, 8470–8479 (2004).

40. Stewart, M. & Fox, S. Do septal neurons pace the hippocampal theta rhythm? *Trends in Neurosciences* (1990).

41. Hangya, B., Borhegyi, Z., Szilagyi, N., Freund, T. F. & Varga, V. GABAergic neurons of the medial septum lead the hippocampal network during theta activity. *The Journal of neuroscience : the official journal of the Society for Neuroscience* (2009).

42. Freund, T. F. & Antal, M. GABA-containing neurons in the septum control inhibitory interneurons in the hippocampus. *Nature* **336**, 170–173 (1988).

43. Fuchs, E. C. *et al.* Local and Distant Input Controlling Excitation in Layer II of the Medial Entorhinal Cortex. *Neuron* (2016).

44. Gonzalez-Sulser, A. *et al.* GABAergic projections from the medial septum selectively inhibit interneurons in the medial entorhinal cortex. *The Journal of neuroscience : the official journal of the Society for Neuroscience* (2014).

45. Takacs, V. T., Freund, T. F. & Gulyas, A. I. Types and synaptic connections of hippocampal inhibitory neurons reciprocally connected with the medial septum. *European Journal of Neuroscience* (2008).

46. Unal, G., Joshi, A., Viney, T. J., Kis, V. & Somogyi, P. Synaptic Targets of Medial Septal Projections in the Hippocampus and Extrahippocampal Cortices of the Mouse. *The Journal of neuroscience : the official journal of the Society for Neuroscience* (2015).

47. Gulyas, A., Hajos, N., Katona, I. & Freund, T. Interneurons are the local targets of hippocampal inhibitory cells which project to the medial septum. *European Journal of Neuroscience* (2003).

48. Toth, K., Borhegyi, Z. & Freund, T. Postsynaptic targets of GABAergic hippocampal neurons in the medial septum-diagonal band of broca complex. *Journal of Neuroscience* (1993).

49. Buzsáki, G. Neural Syntax: Cell Assemblies, Synapsembles, and Readers. *Neuron* **68**, 362–385 (2010).

50. Huxter, J., Burgess, N. & O'Keefe, J. Independent rate and temporal coding in hippocampal pyramidal cells. *Nature* (2003).

51. Harris, K. D. *et al.* Spike train dynamics predicts theta-related phase precession in hippocampal pyramidal cells. *Nature* **417**, 738 (2002).

52. Lisman, J. E. & Jensen, O. The Theta-Gamma Neural Code. *Neuron* **77**, 1002–1016 (2013).

53. O'Keefe, J. & Burgess, N. Dual phase and rate coding in hippocampal place cells: theoretical significance and relationship to entorhinal grid cells. *Hippocampus* (2005).

54. Pastalkova, E., Itskov, V., Amarasingham, A. & Buzsáki, G. Internally Generated Cell Assembly Sequences in the Rat Hippocampus. *Science* **321**, 1322–1327 (2008).

55. O'Keefe, J. & Burgess, N. Geometric determinants of the place fields of hippocampal neurons. *Nature* (1996).

56. Ylinen, A. *et al.* Intracellular correlates of hippocampal theta rhythm in identified pyramidal cells, granule cells, and basket cells. *Hippocampus* (1995).

57. Justus, D. *et al.* Glutamatergic synaptic integration of locomotion speed via septoentorhinal projections. *Nature Publishing Group* (2017).

58. Viney, T. *et al.* Shared rhythmic subcortical GABAergic input to the entorhinal cortex and presubiculum. *eLife* (2018).

59. Joshi, A., Salib, M., Viney, T., Dupret, D. & Somogyi, P. Behavior-Dependent Activity and Synaptic Organization of Septo-hippocampal GABAergic Neurons Selectively Targeting the Hippocampal CA3 Area. *Neuron* (2017).

60. Bolding, K. A., Ferbinteanu, J., Fox, S. E. & Muller, R. U. Place cell firing cannot support navigation without intact septal circuits. *Hippocampus* (2019).

61. Chang, Q. & Gold, P. E. Impaired and spared cholinergic functions in the hippocampus after lesions of the medial septum/vertical limb of the diagonal band with 192 IgG-saporin. *Hippocampus* (2004).

62. Lee, M., Chrobak, J., Sik, A., Wiley, R. & Buzsaki, G. Hippocampal theta activity following selective lesion of the septal cholinergic system. *Neuroscience* (1994).

63. Fraser, K., Poucet, B., Partlow, G. & Herrmann, T. Role of the medial and lateral septum in a variable goal spatial problem solving task. *Physiology behavior* (1991).

64. Galey, D., Durkin, T., Sifakis, G., Kempf, E. & Jaffard, R. Facilitation of spontaneous and learned spatial behaviours following 6-hydroxydopamine lesions of the lateral septum: a cholinergic hypothesis. *Brain research* (1985).

65. Andersen, P. & Moser, E. I. Brain temperature and hippocampal function. *Hippocampus* **5**, 491–498 (1995).

66. FAY, T. & ITH, G. W. OBSERVATIONS ON REFLEX RESPONSES DURING PROLONGED PERIODS OF HUMAN REFRIGERATION. *Archives Neurology Psychiatry* **45**, 215–222 (1941).

67. Robbe, D. & Buzsaki, G. Alteration of theta timescale dynamics of hippocampal place cells by a cannabinoid is associated with memory impairment. *The Journal of neuroscience : the official journal of the Society for Neuroscience* (2009).

Supplementary Material

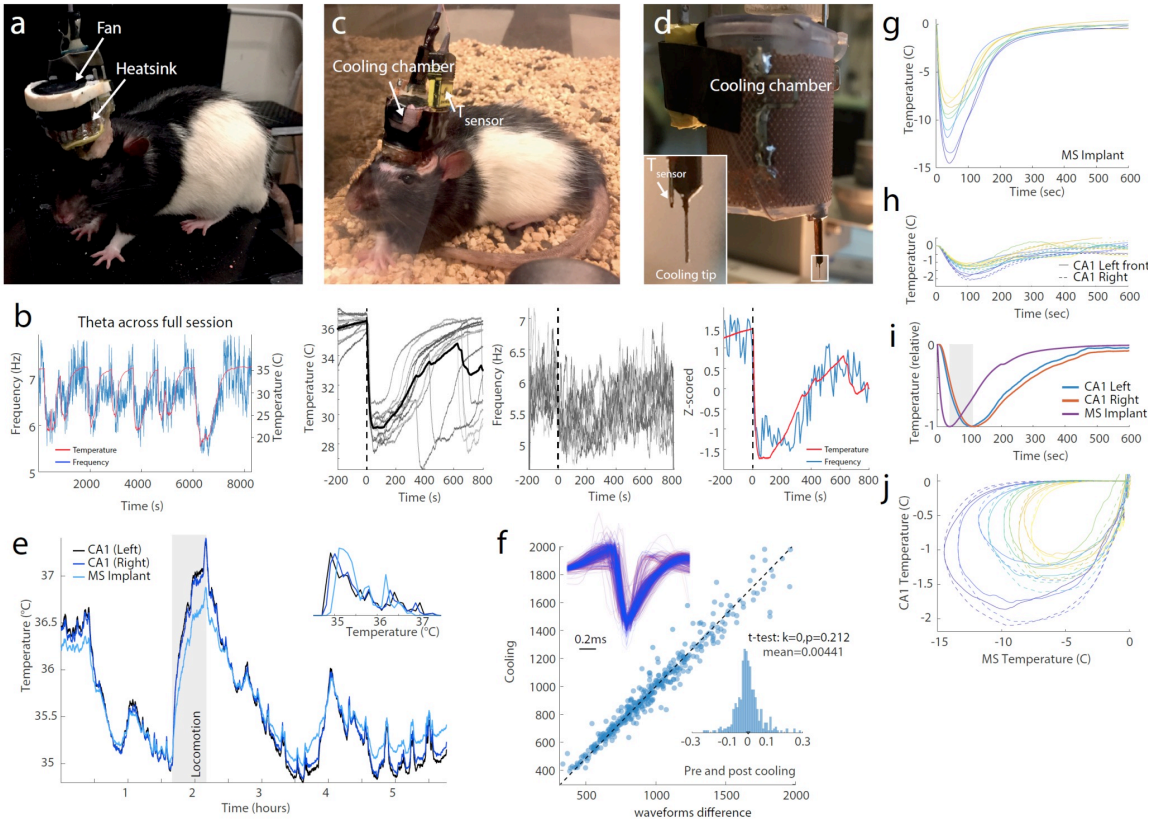

Supplementary Fig. 1. Related to Fig. 2. **Methods of MS cooling.** Two different methods for cooling the cryoprobe were tested. The first one used a Peltier device (panels a; [19]). This allowed precise control of temperature over long duration and performing necessary tests of MS temperature control. However, it required both a heatsink and an electric fan for maintaining stable temperature of the Peltier element, increasing both volume and weight of the device. The second device was a small cooling reservoir (as also shown in Fig. 2a, b). This device was used in all physiological and behavioral experiments. **a**, Photograph of a Peltier device implanted in a rat. On top of the Peltier there is a small, low noise electric fan to cool the device. **b**, Relationship between MS local temperature (red) and theta frequency (blue) in the hippocampus. The MS was repeatedly cooling with dry ice. Second and third panels, successive cooling epochs are superimposed. Fourth panel, superimposed average MS temperature and frequency of hippocampal theta oscillations. Note reliable and non-accommodating relationship between MS temperature and hippocampal theta frequency across several hours. **c**, Photograph of a rat implanted with a dry iced-cooled cryoprobe. **d**, Details of the dry ice container and the cryoprobe with a temperature sensor connected to its outer tube. **e**, Physiological temperature variation in the left and right hippocampus and MS. No cooling was induced in this session. Note that locomotion increases brain temperature (shaded column). Inset: Distribution of time windows spent in each temperature unit. Note >2° C span of temperature variation. **f**, Comparison of hippocampal CA1 unit waveforms before/after (red) and during (blue) MS cooling. Inset histogram shows that MS cooling did not significantly affect unit waveforms. **g**, Magnitude and time course of

MS temperature and simultaneously monitored hippocampal temperature (**h**) in successive cooling sessions in a rat. **i**, Normalized temperature curves. Note the different temporal dynamics and > 50 s delay (shaded area) between the maximum cooling effects in MS and hippocampus. **j**, Lissajous orbit plots illustrate the temporal delays of temperature effects in the MS and hippocampus. Note that the temperature scale for the hippocampus (y) is ~10 times smaller compared to the MS temperature scale (x).

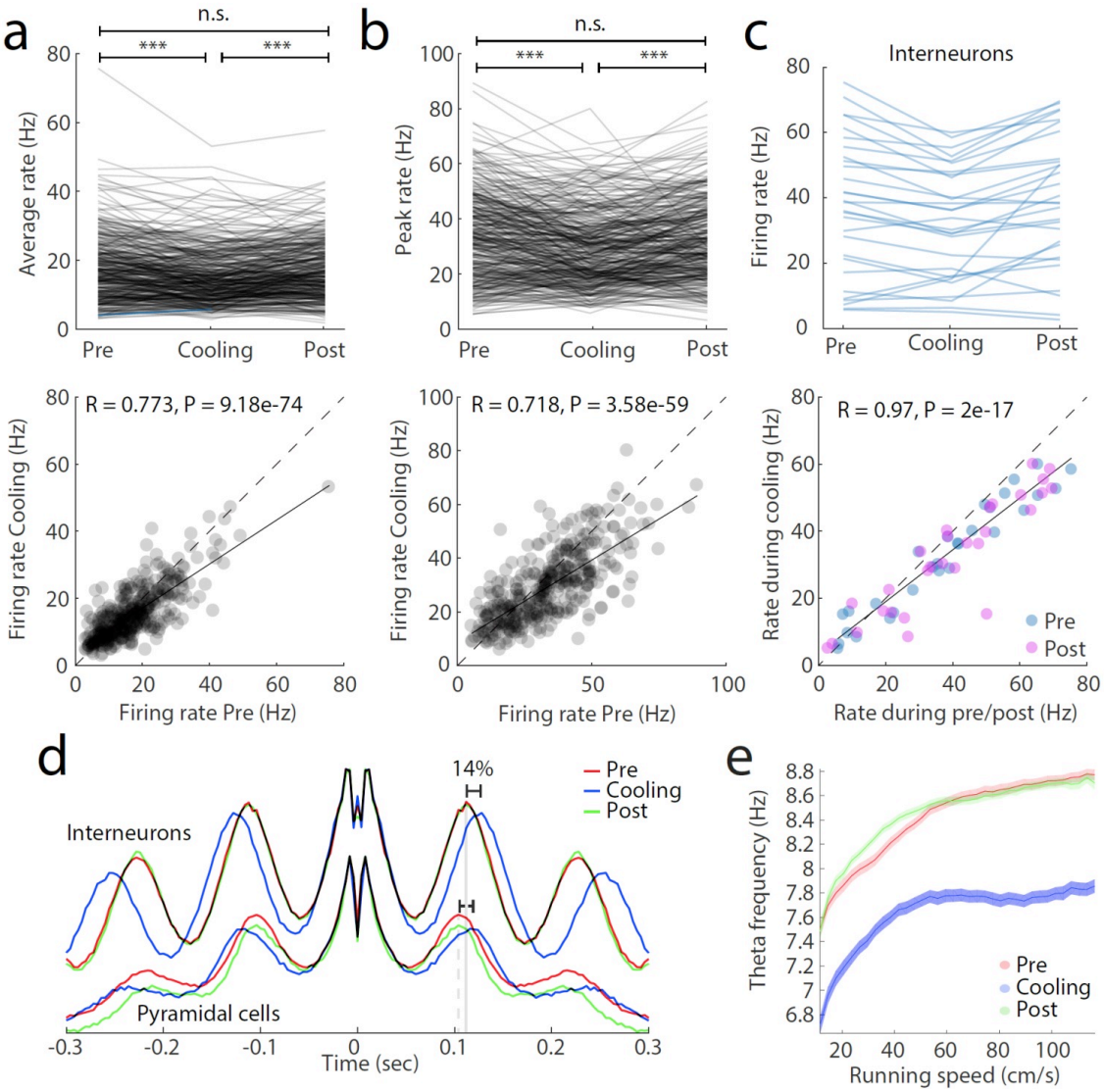

Supplementary Fig. 2. Related to Fig. 3. **MS cooling affects single unit parameters. a**, Firing rates of pyramidal neurons within their place fields (**a**) and their peak firing rates (**b**) (top) and illustration of the rate changes before and during MS cooling. R = 0.7, P < 10^{-58}. **c**, Same display for putative fast firing interneurons. **d**, Autocorrelograms of putative interneurons and pyramidal cells before, during and after MS cooling. Note that pyramidal neurons oscillate faster than interneurons and the theta frequency oscillation of both interneurons and pyramidal cells decreases with MS cooling by approximately 14% on average. The autocorrelograms were constructed from all spikes occurring within place fields during running for pyramical cells, and across the whole maze for

interneurons. **e**, Relationship between running speed and theta frequency as the animals runs through the circular maze, unlike in Figure 3g and h, where the values were obtained from individual place fields.

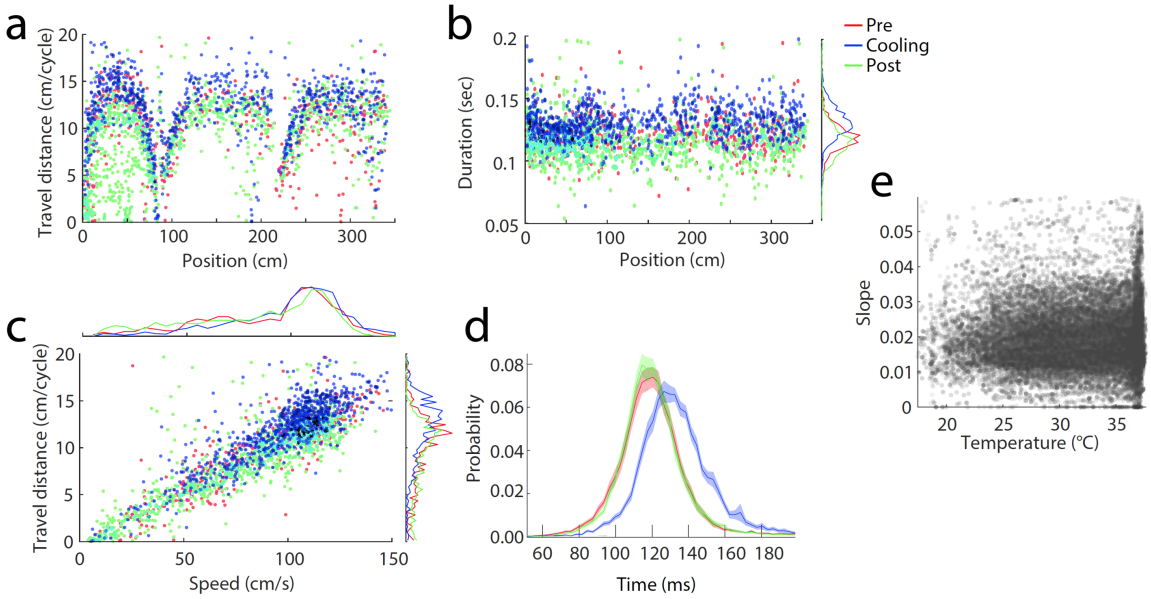

Supplementary Fig. 3. Related to Fig. 3. **Speed and MS cooling affects are dissociable. a**, Distribution of the travel distances per theta cycle during and after MS cooling as a function of the animal's position on the track. 0-75 cm, center arm, followed by runs in the left or right arms of the maze. Note position-dependent variation of travel distances, due to speed variation on the track. **b**, Duration of the theta cycle as a function of the animal's position. Note consistently longer theta duration during MS cooling. Side histograms show longer theta cycles during MS cooling. c. Distance traveled per theta cycle increases with running speed. Top histogram, speed distribution before, during and after MS cooling. This session was chosen for illustration purposes because running speed of the rat remained the same during the entire session. Side histograms show that longer distances are traveled per longer theta cycles during MS cooling. **d**, Distribution of theta cycle duration for all sessions (N = 21). Note that theta cycle duration increased during MS cooling but returned after cooling to the pre-cooling control duration, even though average speed gradually decreased from the beginning to the end of sessions (see Fig. 3e, Fig. 6c). **d**, Phase precession slope as a function of MS temperature. All values from before, during and after MS cooling trials are combined. Note low (R = 0.027) but significant (P = 7.67e-19) correlation.

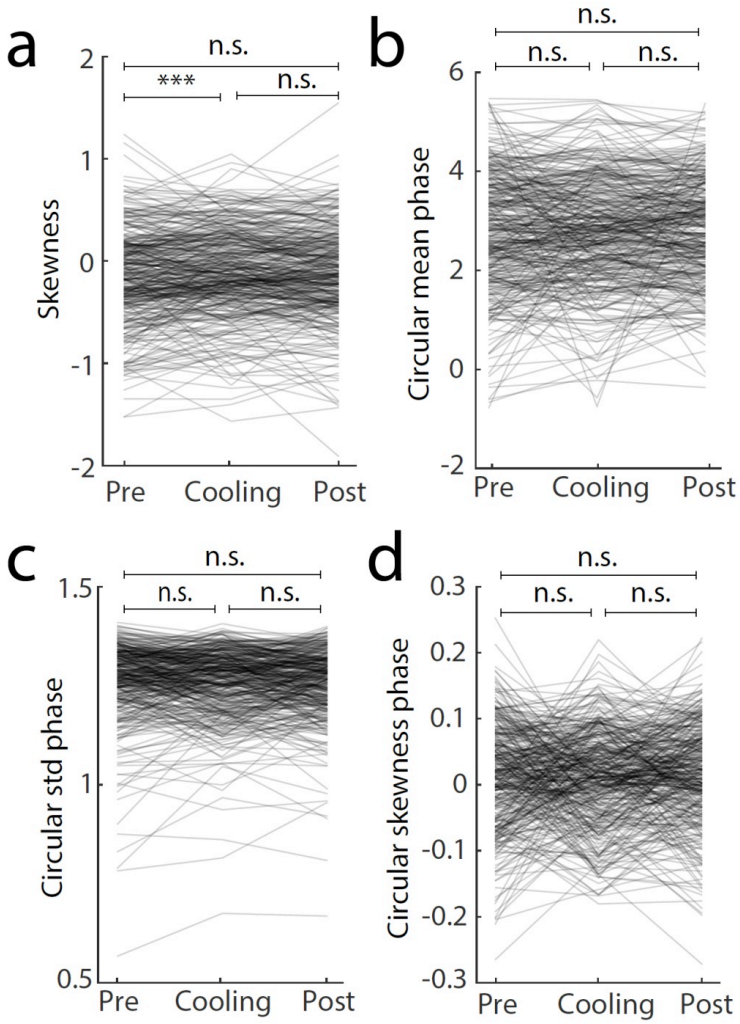

Supplementary Fig. 4. Related to Fig. 4. **Properties of place fields during MS cooling**. **a, b, c, d**, Skewness, mean phase (circular mean phase), standard deviation of phase (circular standard deviation), skewness phase (circular skewness), respectively, as a function of MS cooling.

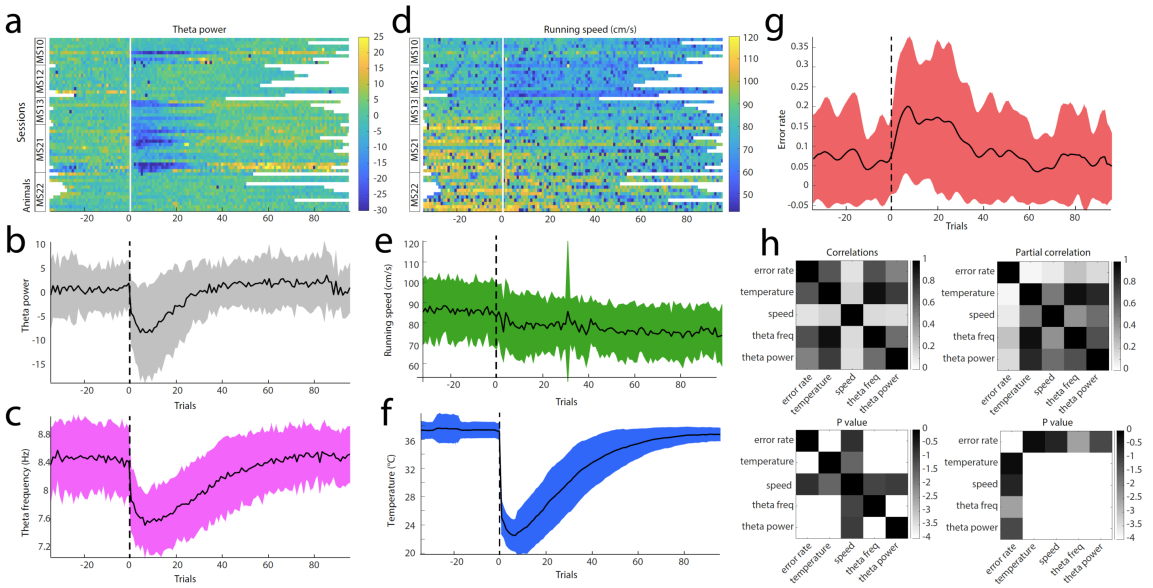

Supplementary Fig. 5. Related to Fig. 6. **Time course of the effects of MS cooling on behavior and physiological parameters**. **a**, **d**, Theta power and running speed as a function of MS cooling trials for each session. **b, e**, Group average and standard deviation related to panels **a** and **d**. Note monotonic deceleration of running speed over the entire session, likely reflecting the decreased motivation of the animal as it consumes more water cumulatively. **c, f**, **g**, Group means of theta frequency, MS temperature and choice errors, respectively. **h**, Correlation values (top) and P values (bottom) for each comparison (left panels). Partial correlation values (top) and P values (bottom) for each comparison (right panels). Note error rates correlate best with theta frequency and have no significant relationship to running speed.

LEAD CONTACT AND MATERIALS AVAILABILITY

Further information and requests for resources and datasets should be directed to and will be fulfilled by György Buzsáki (gyorgy.buzsaki@nyumc.org).

Supplementary Material

METHODS

Subjects and surgery

Rats (adult male Long-Evans, 250-450 g, 3-6 months old) were kept in a vivarium on a 12-hour light/ dark cycle and were housed 2 per cage before surgery and individually after it. All experiments were approved by the Institutional Animal Care and Use Committee at New York University Medical Center.

Animals were anesthetized with isoflurane anesthesia and craniotomies were performed under stereotaxic guidance. A custom designed 3D printed cap (suppl. figure 1a) was attached to the skull with meta-bond, serving as a base for the probe implants and protection. A 12cm x 12cm sheet of copper mesh had beforehand been attached with dental cement to the base, from which a Faraday box/protector cap was later formed. Rats (Table 1) were implanted with silicon probes and tungsten wires to record local field potential (LFP) and spikes from the CA1 pyramidal layer [11]. The tip of the cooling device was implanted at AP: +0.8mm, ML: 0.6mm (tilted 6° towards the midline), and lowered 6 mm below the brain surface, after which it was attached to the skull and base.

Silicon probes (NeuroNexus, Ann-Arbor, MI and Cambridge Neurotech, Cambridge, UK) were implanted in the dorsal hippocampus (antero-posterior (AP) -3.5mm from Bregma and 2.5 mm from the midline along the medial-lateral axis (ML)). The silicon probes consisted of three designs (table q): 4-shank with 16 sites each shank in a poly 3 staggered, 5-shank with 12 sites each shank in a staggered configuration, and 6-shank probe with 10 sites each shank (Figure 2B). They were mounted on custom-made micro-drives to allow their precise vertical movement after implantation (Vandecasteele et al., 2012). Probes were implanted above the target region by attaching the micro-drives to the skull with dental cement. Craniotomies were sealed with sterile wax or gel. Stainless steel screws or 100µm steel wires were bilaterally screwed or implanted above the cerebellum, serving as ground and reference electrodes, respectively, for electrophysiological recordings. At the end of electrode implantation and cryoprobe implantation (see below), the copper mesh was folded upwards, connected to the ground screw, and painted with dental cement. The mesh acts as a Faraday cage, shielding the recordings from environmental electric noise and muscle artifacts, provides structural stability and keep debris away from the probe implants. After post-surgery recovery, probes were moved gradually in 50 to 150 µm steps until they reached the CA1 the pyramidal layer. The pyramidal layer of the CA1 region was identified by physiological markers: increased unit activity, strong theta oscillations and phase reversal of the sharp wave ripple oscillations (Mizuseki et al., 2011).

Cooling devices

Two different cooling techniques were used. A Peltier device and dry ice in Styrofoam chamber ('dry ice cryoprobe'). Both cooling devices were attached to a silver wire that conducted cooling to the medial septum (Fig. 2a).

Dry ice cryoprobe

A 15mm diameter 3D printed container with lid was constructed and a hollow cylinder made from Styrofoam (outer diameter: 18mm, inner diameter: 10mm) was inserted into the container. A 20 mm silver wire (127µm diameter, a-m systems, #781500), wrapped with graphene sheet (50µm thickness), was inserted through the base of the styrofoam container and attached to the inside of the chamber with thermal adhesive (Arctic Silver Thermal Adhesive, ASTA-7G). 10mm of the wire was protruding from the base of the chamber. The protruding wire was then inserted into an 8 mm long hollow polyimide tube (1 mm diameter), such that 1.5mm of the silver wire was exposed. The polyimide

tube was further sealed with thermal adhesive in both ends to create an air vacuum around the silver wire (figure 2A). The air vacuum served as a thermal isolation, to minimize the cooling effects along the wire (Aronov and Fee, 2011). Finally, a thermocouple (a temperature sensor) was attached with epoxy adhesive to the cooling implant with the tip of the probe aligned with the protruding silver wire (figure 2A, and suppl. figure 1A). Cooling with dry ice was achieved by placing a small amount of dry ice into the "cooling chamber", which conducted the cooling to the exposed implanted silver wire.

Peltier cooling device

The hot side of a two-stage Peltier device (custom thermoelectric , 04812-5L31-04CFG 2 Stage Thermoelectric/Peltier Module) was attached to a copper heatsink (5mm x 5 mm, Enzotech MOS-C10 Forged Copper MOSFET Heatsinks) with heat-conductive adhesive (Arctic Silver, Arctic Silver Thermal Adhesive). The heatsink was shaped to fit the inner dimensions of a 25 mm x 25 mm electric fan (GDSTIME, 5V DC Brushless fan). An 18 mm long silver wire (200µm diameter, a-m systems #782000) was attached to the cold side of the peltier device with heat conductive adhesive. A 8mm long polyimide tube (1.1 mm diameter, Cole-Parmer 95820-09) was attached around the silver wire, sealed, and a temperature sensor was attached to the tube. 1.5mm of the silver wire was exposed at the tip of the cooling device.

Electrophysiological Recordings

Animals were handled daily and accommodated to the experimenter before surgery. They were water restricted for 22 hours and trained to perform the behavioral task prior to surgery. After recovery from surgery, the animals were water restricted again to perform a spatial alternation task in the 'theta' (figure 8-shape) maze. The behavior session typically lasted 40 min, consisting of 40 control trials, after which the cooling was applied by manually placing a small amount of cry ice in the cooling chamber. The cooling typically peaked after about 60 sec after the cooling onset (suppl. fig. 1G) and lasted for about 10-12 minutes, corresponding to approximately 50 trials (figure 6C and suppl. Figure 2). The animal would continue the task for a total number of trials ranging from 80 to 200 (mean: 150 trials). The behavior was preceded and followed by 1-3 hours sleep sessions in the home cage of the rat.

Memory-demanding alternation task in a theta maze

In a 'theta' (or figure 8) maze (110 cm diameter, Fig. 2c), animals were trained to alternate between the left and the right arms to receive water drops at the reward locations (Figure 2C). The maze was placed on a platform 1 meter above the floor. The rat started from the reward location, ran along the central arm, after which it chose to run along the left or the right arm. If the animal performed the alternation correctly (opposite arm than they visited in the previous trial), it received water reward. If it chose the wrong direction, the path to the reward location was blocked and the rat was forced to run back along the correct arm to collect reward.

The position of the animal was tracked with an OptiTrack 6-camera system (Natural Point Corp.). Calibration across cameras allowed for a three-dimensional reconstruction of the animal´s head position and orientation. A rigid body was created by mounting 6 reflective markers to a small 3D-printed holder, attached to the animal´s head-cap and tracked simultaneously by 6 infrared cameras (OptiTrack Flex 3 cameras) at 120Hz.

Animal	Recording implant	Manipulation implant	Behavioral protocol
MS6	5×50µm Single wires in CA1	Dry ice cryoprobe in MS	Wheel box
MS7	1×50µm Single wires in MS, 4×50µm Single wires in CA1	Dry ice implant in MS	Wheel box
MS8	5×50µm Single wires in MS 3×50µm Single wires in CA1	Peltier thermal device in MS	Wheel box
MS9	Cambridge Neurotech P1-64ch, 4 shanks, poly 2, CA1	Peltier thermal device in MS	Theta maze, wheel box
MS10	NeuroNexus Buzsaki 5×12	Dry ice cryoprobe in MS	Theta maze, wheel box
MS12	NeuroNexus Buzsaki 5×12 in CA1 in both hemispheres	Dry ice cryoprobe in MS	Theta maze, wheel box
MS13	Cambridge Neurotech P1-64ch, poly 2, in CA1 in both hemispheres	Dry ice cryoprobe in MS	Theta maze, wheel box
MS21	2 x NeuroNexus Buzsaki64sp, 6 shank, 10 staggered sites, implanted in CA1 bilaterally	Dry ice cryoprobe in MS	Theta maze, linear track, wheel box
MS22	2 x NeuroNexus Buzsaki64sp, 6 shank, 10 staggered sites, implanted in CA1 bilaterally	Dry ice cryoprobe in MS	Theta maze, linear track, wheel box

Table 1: Animal implants and behavioral protocols

QUANTIFICATION AND STATISTICAL ANALYSIS

Electrophysiological recordings were conducted using an Intan recording system: RHD2000 interface board with Intan 64 channel preamplifiers sampled at 20 kHz (Intan Inc).

Spike Sorting

Spike sorting was performed semi-automatically with KiloSort (Pachitariu et al. 2016) https://github.com/cortex-lab/KiloSort), using our own pipeline KilosortWrapper (a wrapper for KiloSort, DOI; https://github.com/brendonw1/KilosortWrapper), followed by a manual curation using the software Phy (https://github.com/kwikteam/phy) and our own designed plugins for phy (https://github.com/petersenpeter/phy-plugins).

Unit Classification

Well isolated units were classified into putative cell types using the Cell Explorer

(DOI:10.5281/zenodo.3368763; https://github.com/petersenpeter/Cell-Explorer). Three cell types were assigned: putative pyramidal cells, narrow spike interneurons and wide spike interneurons. Spiking characteristics, including the autocorrelograms, spike waveforms and putative monosynaptic connections derived from short-term cross-correlograms were used to select and characterize well-isolated units and separate them into pyramidal cell and interneuron classes.

Theta phase and phase precession

An LFP channel located in the CA1, was filtered in the theta range (4-10Hz, third order butter filter, filt-filt), and translated into phase by the Hilbert transform. The phase precession slope of a place field, was determined by performing a circular-linear regression on the position vs theta phase for all spikes within the boundaries of the place field.

Oscillation Frequency of Neurons

For quantifying oscillation frequency of neurons, a 1ms-resolution spike raster was created and convoluted with an 80-point gaussian window. The auto-correlogram was calculated and the peak between 50ms and 150ms was determined and its reciprocal value was regarded as the oscillation frequency. For place field analysis (e.g. Fig. 3 B,C,F,H), only the spikes emitted as the animal passed through the field was included.

Place cell analysis

Spiking data were binned into 3-5 cm wide segments of the maze, generating the raw maps of spike number and occupancy probability. Place field boundaries were manually defined by the following criteria: a spatial tuned firing rate, phase precession, and peak firing rate above 10Hz. For figure 5, place fields were automatically defined by the following criteria: at least 4 bins, where the firing rate was above 10% of the peak rate in the maze, peak firing rate > 8 Hz and spatial coherence > 0.6 (Muller et al., 1989; Hafting et al. 2008).

Spatial temporal compression

To determine the spatial-temporal compression, the distance between pairs of fields (determined as the spatial distance between the spatial peak firing rate) was plotted against the temporal delay inside theta cycles (either time or phase).

The temporal offset between individual overlapping fields was determined with a 1ms bin-sized cross correlogram, convoluted with a 60 bin-wide gaussian window. The phase offset was determined with a 0.01π bin-sized cross correlogram convoluted with a 60 bin-wide gaussian window. The compression and oscillation period were determined by fitting the surface equation below to the density of points (fig 5c):

$$Z = \cos\left(x\frac{2\pi}{a \cdot b} + y\frac{2\pi}{b} + 1\right) \cdot exp\left(-(x + f \cdot y)^{2/2c^2}\right) \cdot \exp\left(-(y - g)^{2/2d^2}\right) \cdot e$$

Where a is the compression index (slope), b the period (inverse of the oscillation frequency), c and d the widths of the two gaussian envelopes along the x and y dimensions, e the amplitude, f the x-y shift and g the y-offset.

Statistical Analyses

All statistical analyses were performed with MATLAB functions or custom-made scripts. For rank order calculation, the probability of participation and firing rate correlations, the unit of analysis was single cells. Unless otherwise noted, for all tests, non-parametric two-tailed Wilcoxon rank-sum (equivalent to Mann-Whitney U-test), Wilcoxon signed-rank or Kruskal-Wallis one-way analysis of variance were used. Due to experimental design constraints, the experimenter was not blind to the manipulation performed during the experiment.

DATA AND CODE AVAILABILITY

The dataset will be available from our data share via our website

https://buzsakilab.com/wp/resources/.

KEY RESOURCES TABLE

Resource	Source	Identifier/Location	Description
SUBJECTS			
Rat: Long-Evans	Charles River	Cat#: Crl:LE 006	9 male adults
DATA			
Hippocampal data	Peter C. Petersen & Gyorgy Buzsaki	https://buzsakilab.com/wp/resources/	Public data share with data from our lab
SOFTWARE			
Cell Explorer	Peter C. Petersen & Gyorgy Buzsaki	https://github.com/petersenpeter/Cell-Explorer http://doi.org/10.5281/zenodo.3368763	Cell classification pipeline and GUI built in Matlab
KiloSort	Pachitariu M & Cortex-lab	https://github.com/cortex-lab/KiloSort	Template based spike sorting Matlab software

KilosortWrapper	Peter C. Petersen & Brendon Watson	https://github.com/brendonw1/KilosortWrapper	A wrapper for KiloSort written in Matlab
Phy	Cyrille Rossant, Ken Harris et al.	https://github.com/cortex-lab/phy	Python GUI for manual spike curation
Phy plugins	Peter C. Petersen	https://github.com/petersenpeter/phy-plugins	Plugins for phy
MATLAB	MathWorks	https://www.mathworks.com/	
Buzcode	Buzsaki Lab	https://github.com/buzsakilab/buzcode	Matlab analysis tools
FMA Toolbox	Michaël Zugaro	http://fmatoolbox.sourceforge.net/	A Matlab toolbox for Freely Moving Animal (FMA)
OTHER			
Silicon probe (5x12, 6x10)	NeuroNexus	https://neuronexus.com/	
Silicon probe (4x16)	Cambridge Neurotech	https://www.cambridgeneurotech.com/	
Intan RHD2000	Intan technologies	http://intantech.com/RHD2000_evaluation_system.html	
Motive tracking system	Optitrack	http://optitrack.com/	6 Flex3 camera system

Method reference list

English, D., McKenzie, S., Evans, T., Kim, K., Yoon, E., and Buzsáki, G. (2017). Pyramidal Cell-Interneuron Circuit Architecture and Dynamics in Hippocampal Networks. Neuron *96*, 505-520.e7.

Hafting, T., Fyhn, M., Bonnevie, T., Moser, M.-B., and Moser, E.I. (2008). Hippocampus-independent phase precession in entorhinal grid cells. Nature *453*, 1248.

Muller, R., and Kubie, J. (1989). The firing of hippocampal place cells predicts the future position of freely moving rats. J Neurosci *9*, 4101–4110.

Pachitariu, M., Steinmetz, N., in Neural, K.S., and 2016 Fast and accurate spike sorting of high-channel count probes with KiloSort. Papers.Nips.Cc.

Vandecasteele, M., S, M., Royer, S., Belluscio, M., Berényi, A., Diba, K., Fujisawa, S., Grosmark, A., Mao, D., Mizuseki, K., et al. (2012). Large-scale recording of neurons by movable silicon probes in behaving rodents. J Vis Exp Jove e3568.

Mizuseki, K., Diba, K., Pastalkova, E. & Buzsáki, G. Hippocampal CA1 pyramidal cells form functionally distinct sublayers. *Nat Neurosci* **14**, 1174–1181 (2011).

Acknowledgements

We would like to thank Andrew Maurer, Viktor Varga, Manuel Valero and Antonio Fernandez-Ruiz for helpful comments on the manuscript. This work was supported by the Independent Research Fund Denmark, Lundbeckfonden Denmark, NIH, MH54671, MH107396, and NS 090583, NSF PIRE grant (#1545858), U19 NS107616 & U19 NS104590.

Author Contributions

GB and PP designed the experiments. PP performed the experiments and analyzed the data. GB and PP wrote the paper.

Declaration of Interests

The authors declare no competing interests.